

VALIDATION OF A LOW-COST DATA ACQUISITION SYSTEM FOR AIRCRAFT VIBRATION TESTING

Gabriele Dessena [1], Andrea Dell'Edera [2], Francesco M.A. Mitrotta [1,3] & Oscar E. Bonilla-Manrique [4]

[1]Department of Aerospace Engineering, Universidad Carlos III de Madrid, Avenida de la Universidad 30, Leganés, 28911, Madrid, Spain
[2]Department of Mechanics, Mathematics and Management, Politecnico di Bari, Via E. Orabona 4, 70126, Bari, Italy
[3]School of Civil, Aerospace, and Design Engineering, University of Bristol, University Walk, Bristol BS8 1TR, UK
[4]Electronic Technology Department, Universidad Carlos III de Madrid, Avenida de la Universidad 30, Leganés, 28911, Madrid, Spain

Abstract

Experimental vibration testing of aircraft structures depends critically on the quality of the data acquisition system (DAQ), yet commercial instrumentation remains costly for early-stage research programmes and lightweight platforms. This work validates an affordable and modular DAQ system, built around Orange Pi 3 LTS single-board computers and Adafruit LSM6DS3TR-C MEMS inertial measurement units under a Python-based master–slave architecture, against a Siemens Testlab system with PCB Electronics IEPE accelerometers on a small fixed-wing UAV. Three test configurations are considered: ambient vibration testing (AVT), taxi vibration testing (TVT), and impact hammer testing, the latter providing the reference dataset from industry-grade instrumentation. Three structural modes are identified in the 0–25 Hz band, with frequency deviations and Modal Assurance Criterion consistent with different test setups for the same structures. The total hardware cost is below €600, confirming that the system is adequate for structural modal identification within its operating bandwidth.

Keywords: Aircraft Vibration Testing, Low-cost Data Acquisition, Modal Analysis, Taxi Vibration Testing, Ambient Vibration Testing

1. Introduction

Experimental vibration testing is a fundamental activity in aircraft structural dynamics, supporting modal identification, numerical model validation, and the assessment of dynamic behaviour under both operational and controlled excitation [1]. Data acquisition systems (DAQs) constitute the primary interface between physical phenomena and their digital representation, and their accuracy, repeatability, and channel consistency directly determine the quality of any subsequent analysis [2]. In aerospace applications, this dependency is consequential: Ground Vibration Tests (GVTs) [3], Taxi vibration tests (TVTs) [4], and Ambient Vibration Tests (AVTs) [5] all rely on acceleration data whose integrity cannot be recovered at the post-processing stage if the measurement chain introduces systematic errors or timing inconsistencies. Notably, we can divide these three into Operational [2], as TVT and AVT, and Experimental [6], as GVT, Modal Analysis (OMA and EMA). This distinction is based solely on the fact that in EMA both input and output can be measured, while in OMA only the output can.

Commercial vibration measurement platforms offer high accuracy, calibrated sensitivity, and advanced signal conditioning; however, their cost, logistical complexity, and integration requirements

https://doi.org/10.71945/icas2026_0724

often preclude their use in early-stage testing campaigns, research-oriented programmes, and experiments conducted on lightweight or expendable platforms [7]. This gap has sustained growing interest in DAQ solutions based on Single-Board Computers (SBCs) and Micro-Electro-Mechanical Systems (MEMS) Inertial Measurement Units (IMUs), which offer a practical route to multi-channel, distributed acceleration measurement at a fraction of the cost of conventional (IEPE – Integrated Electronics Piezo-Electric) instrumentation.

A comprehensive review of MEMS-based wireless accelerometer boards for vibration-based Structural Health Monitoring in [8] establishes that the performance gap relative to conventional IEPE transducers does not preclude reliable identification of low-to-mid-frequency (at least the 0-200 Hz frequency band) structural modes. The same pattern has since been confirmed in field deployments on civil infrastructure. Notably, in [9], a purpose-built MEMS accelerometer system is benchmarked against PCB 607A61 piezoelectric sensors during an ambient vibration campaign on an in-service highway bridge, accurately recovering the modes of interest. In the aerospace domain specifically, recent contributions have demonstrated this trend across different platforms and sensing strategies. A Raspberry Pi-based system employing MEMS accelerometers is developed for Unmanned Aerial Vehicle (UAV) GVT in [10]. Moreover, an Arduino-based DAQ using time-of-flight sensors is proposed for real-time wing vibration displacement measurement in [11]. MEMS gyroscopes are investigated as an alternative measurement quantity for modal parameter tracking and aeroelastic stability monitoring in flutter tests [12], and Raspberry Pi-compatible Inertial Measurement Units (IMUs) are deployed on a high aspect ratio wing spar for nonlinear modal analysis, where their mass loading effect on the nonlinear dynamic response is ivestigated [13]. Taken together, these contributions indicate that open-hardware platforms can resolve the dominant spectral content of aerospace vibration phenomena, provided that their limitations in sampling rate, noise floor, and inter-channel synchronisation are acknowledged and accounted for in the experimental design.

A preliminary version of this system was introduced in [14], where its design and initial experimental validation is veriefied through the qualitative comparison of TVTs and AVTs response spectra on a small fixed-wing UAV. That study confirmes consistent spectral repeatability across multiple test runs; however, validation was conducted without a calibrated reference system, and no comparison against industry-standard instrumentation was performed. This work addresses that limitation directly. The validation campaign is extended to include a classical impact hammer test carried out with a Siemens Testlab data acquisition system[1] and PCB Electronics IEPE accelerometers[2], providing a controlled reference dataset for modal identification against which the low-cost system can be assessed. The central question is whether the affordable system recovers the same dominant spectral features as industry-standard instrumentation, and to what degree of agreement.

2. Materials and Methods

2.1 Low-Cost Acquisition Hardware Architecture

The DAQ system is built around a distributed master–slave architecture in which each acquisition module consists of an Orange Pi 3 LTS single-board computer (SBC) interfaced with multiple Adafruit LSM6DS3TR-C six degrees-of-freedom (DoF) MEMS IMUs, with address conflicts among identical sensors resolved through an Adafruit PCA9548A eight-channel I^2C multiplexer. The SBC provides the local processing and communication capability for each node, whilst the IMUs supply three-axis acceleration measurements at configurable output data rates and measurement ranges. The selection of these components is driven by their low unit cost, compact form factor, and compatibility with standard I^2C communication, which together satisfy the design requirement of a deployable, multi-channel system at minimum hardware expenditure. The key specifications of all three hardware components are summarised in Table 1.

[1] https://www.siemens.com/en-us/products/simcenter/simulation-test/data-acquisition-systems/

[2] https://www.pcb.com/sensors-for-test-measurement/accelerometers/general-purpose

[3] http://www.orangepi.org/html/hardWare/computerAndMicrocontrollers/details/orange-pi-3-LTS.html

[4] https://www.adafruit.com/product/4503

[5] https://www.adafruit.com/product/5626

Table 1 – Hardware component specifications.

Parameter	**Orange Pi 3 LTS**[3] **– (SBC)**	**LSM6DS3TR-C**[4] **– (IMU)**	**PCA9548A**[5] **– (Multiplexer)**
Manufacturer	Xunlong Software	STMicroelectronics	Texas Instruments
Processor / IC	Allwinner H6 Cortex-A53, 1.8 GHz	—	—
Sensing axes	—	3-axis accel. + 3-axis gyro	—
Accel. full scale	—	±2–±16 g	—
Gyro full scale	—	±125–±2000 dps	—
Output data rate	—	12.5 Hz – 6.66 kHz	—
ADC resolution	—	16-bit	—
I^2C channels	—	1 (fixed address)	8 bidirectional
I^2C clock	Up to 400 kHz	Up to 400 kHz	0–400 kHz
RAM / Storage	2 GB / 8 GB eMMC	—	—
Wireless	Wi-Fi 5, BT 5.0	—	—
Supply voltage	5 V (USB-C)	1.71–3.6 V	2.3–5.5 V
Operating temp.	0 to +70 °C	−40 to +85 °C	−40 to +85 °C
Dimensions	56×85 mm	2.5×3×0.83 mm (IC)	—
Mass	45 g	1.7 g	5.1 g
Unit cost (approx.)	€90 – USD 80	€7.50 – USD 9.95	€6 – USD 6.95

The multiplexer is interposed between each SBC and its connected IMU array. It selectively activates individual sensor channels, effectively isolating each IMU on a separate logical bus whilst retaining a single physical I^2C interface to the SBC. This arrangement allows multiple identical sensors to operate concurrently without hardware modification and without introducing additional communication interfaces.

In the master–slave layout, each slave module is responsible for local sensor initialisation and data acquisition. The master unit coordinates the network: It broadcasts acquisition parameters to all slave modules prior to each test, ensuring consistent configuration across the sensor array, and receives the data streams transmitted by each slave during acquisition. Data acquired by the slave modules is streamed to the master in real time rather than being buffered locally until test completion, which reduces per-node memory demand during the acquisition process. Upon reception, the master unit organises the incoming data and writes it to comma-separated values (CSV) files for subsequent post-processing. The software framework of this architecture is implemented in Python and is described in detail in [14]. The specific acquisition parameters and sensor placement adopted in the present validation campaign are discussed in Section 2.3.

The configuration validated in this work comprises one master and two slave modules; each slave can connect to up to four IMUs and transmitting acceleration data along the x, y, and z axes. The number of IMUs per slave node and multiplexer is limited by the I^2C bandwidth. Communication between master and slave nodes is carried out over a local wireless network via the Internet Protocol (IP), with each SBC assigned a fixed IP address. The resulting system architecture is illustrated in Figure 1.

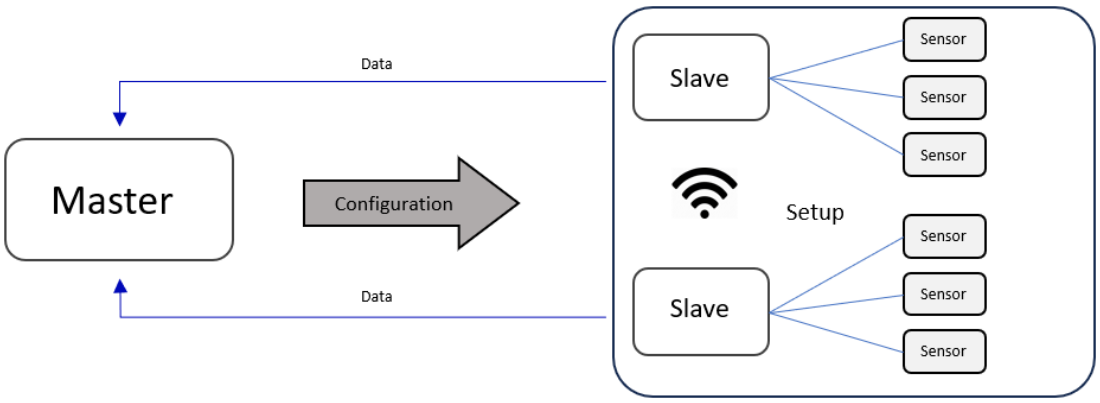


Figure 1 – Block diagram of the low-cost-acquisition system (retrieved from [14][6]).

2.2 The Volantex RC Ranger 2400

The test article considered in this validation campaign is the Volantex RC Ranger 2400[7], a commercially available fixed-wing UAV designed as a first-person-view (FPV) / UAV carrier platform shown in Figure 2.



Figure 2 – Volantex Ranger 2400 resting before a flight at Club Ícaro in Leganés, Spain.

The airframe is characterised by a 2.4 m wingspan and an overall fuselage length of 1.23 m, with an empty structural mass of approximately 1.7 kg, exclusive of the battery pack. The wing is made by EPO (Expanded Polyolefin) foam structurally reinforced with two carbon fiber spars embedded internally along the main wing structure. Metal rods are used to secure and bridge the detachable half wing directly to the fuselage. The fuselage features a unibody plastic construction (blow-molded with plywood formers) that provides crash resistance and a large internal cavity suited to the carriage of payloads or auxiliary battery packs. The wing geometry incorporates a dedicated high-lift aerofoil section selected to sustain elevated payload fractions, a characteristic consistent with the platform's intended UAV carrier role. In the plug-and-play (PNP) configuration adopted for this study, the aircraft is equipped with an outrunner brushless motor driving a 10-inch propeller, regulated by a 40 A switch-mode battery eliminator circuit electronic speed controller, and actuated by six 9-gram servos governing a control surface layout that includes ailerons, rudder, elevator, and flaps. The nominal endurance under standard conditions is approximately 40 minutes with a recommended 14.8 V, 2700 mAh lithium polymer battery; although the battery is not included for the tests considered in this work. The moderate structural mass, large wingspan, and a geometrically simple wing-dominated planform, make the Ranger a suitable and repeatable test article for experimental vibration studies. Even more, since the dominant structural modes are expected to manifest within the frequency band resolvable by MEMS-based acquisition systems, as discussed in Section 1. and shown for a similar system in [15].

2.3 Hammer, Ambient, and Taxi Vibration Testing

In this work, three different types of vibration tests are considered to validate the proposed acquisition system.

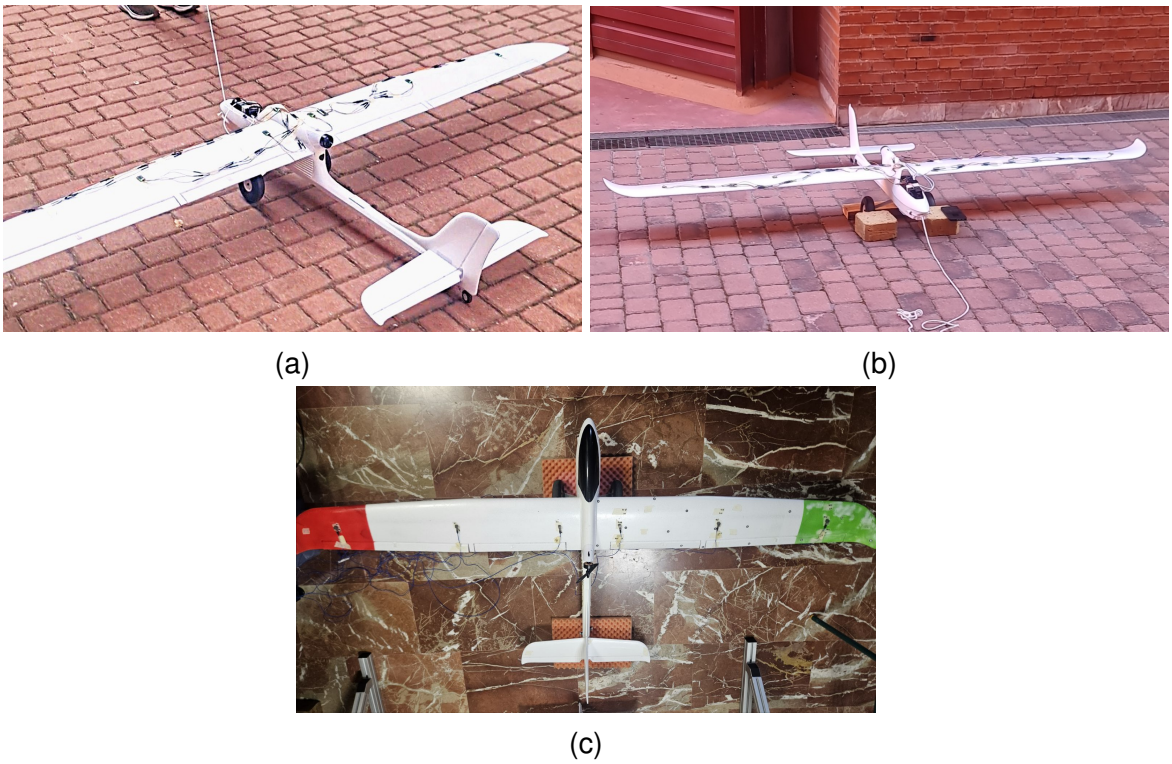
Hammer testing is the procedure in which a structure is excited with an impulse. Typically, the forcing is one or more modal hammer taps, which induce a free-decay-like response. In this test, both input and output are recorded, such that this test can be classified as EMA.

On the other hand TVT and AVT fall under the OMA domain, despite having clear differences. AVT, as per the name, uses the ambient-induced vibration, assumed to be White Gaussian Noise (WGN), as an excitation source for the structure. This has the main advantage of not requiring any expensive

[6]Please note that all material that has been retrieved from [14] comes from its preprint [https://arxiv.org/abs/2601.07783].

[7]https://www.volantexrc.eu/volantex-rc-ranger-2400-professional-fpv-uav-carrier-757-9-pnp-p-308.html

excitation gear and setups, but fails to properly excite higher frequency bands. While this approach is mostly used for the vibration monitoring of heritage and civil buildings [16], it has been successfully employed in Aeronautical structures too [17].
Finally, TVT is an OMA procedure where the aircraft either taxies under its own power or its towed and the imperfections on the taxiway tarmac excite the structure. In this case, the input is assumed to WGN too. The Ranger under TVT, AVT, and hammer test conditions is shown in Figure 3.



(a) (b)

(c)

Figure 3 – Ranger during (a) TVT, (b) AVT, and (c) hammer test. (a) and (b) are retrieved from [14]).

In order to carry out the system validation, two testing campaigns on the Ranger are run: the first involves TVT and AVT, and the latter involves hammer testing. In the TVT and AVT, the aircraft is equipped with only the proposed low-cost data acquisition system, while industry-standard IEPE accelerometers are used for the hammer test. Specifically for the hammer test, the Ranger wing is instrumented with six PCB Piezotronics 333B30[8] uniaxial accelerometers with a sensitivity of ≈100 mVg^{-1} and a mass of 4g. The structure is excited with the PCB Piezotronics Model 086C03[9] modally tuned hammer (sensitivity: 2.25 mVN^{-1}) with a single tap on the near root wing lower surface. Notably, the accelerometers, both the industrial-grade and the low-cost alternative, are placed in the same positions along the wing. This is shown in Figure 4, while the exact coordinate locations are in Table 2.

Table 2 – Sensor Position w.r.t. the frame of reference in Figure 4.

Sensor No.	0_1	1_1	2_1	0_2	1_2	2_2
x [cm]	−8.6	−8.6	−8.6	−8.6	−8.6	−8.6
y [cm]	8.6	52.6	97.6	−8.6	−39.2	−96.6

The sensor layout adopted for this campaign is not designed to retrieve a specific number of modes, nor is it optimised for any particular modal target, but solely for the functional verification and validation of the DAQ system. The chosen spanwise inline arrangement does not allow for the direct

[8] https://www.pcb.com/products?m=333b30
[9] https://www.pcb.com/products?m=086c03

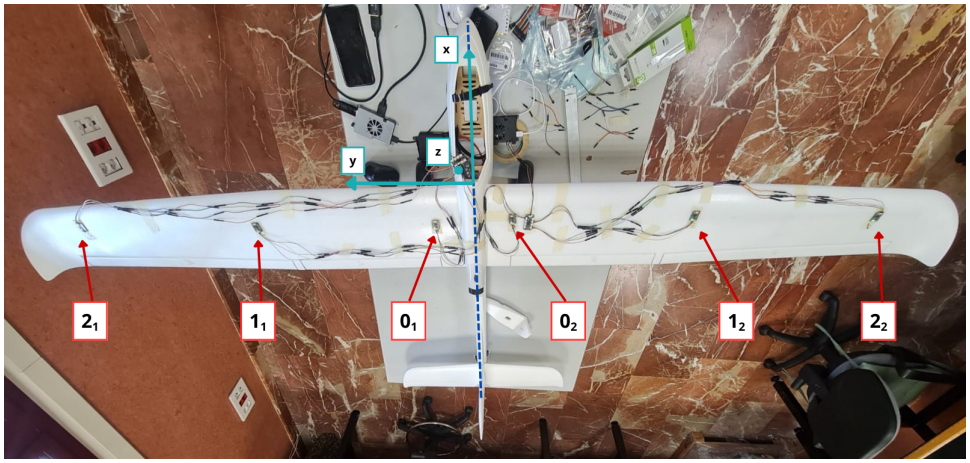


Figure 4 – Sensor layout on the small fixed-wing UAV (retrieved from [14]).

identification of torsional deformation, as resolving torsion requires measurements at a minimum of two chord positions to capture the chordwise gradient. However, the low-cost IMU are triaxial and provide measurement along all three axes, which allows both out-of- and in-plane bending modes to be observed from the same sensor locations.

The industrial-grade setup of the hammer test – from now on referred to as EMA, for brevity – is completed by a Simcenter SCADAS[10] connected to the Siemens Testlab 2013 software for data collection, sampled at $f_s = 1024$ Hz. FRFs are estimated using the H1 estimator over a 400 Hz analysis bandwidth, with a frequency resolution of 0.5 Hz. The low-cost acquisition system, used for TVT and AVT, is set to $f_s = 200$ Hz, which resolves the signal up to 100 Hz by the Nyquist criterion.

The TVT is repeated 8 times, and each lasts 60 s, while the AVT is repeated 2 times, each lasting 20 minutes. Concerning the hammer test, the results are averaged from the acquisition of five taps, with the recording lasting until the free decay is completed. Notably the data acquired from TVT and AVT are processed to retrieve the sampling frequency of 200 Hz, as the sensors send the data at a given rate close to the requested sample frequency, not exactly at 200 Hz. To solve this, the signal was linearly interpolated and extrapolated in MATLAB to retrieve a sampling frequency of 200 Hz. No such issues are encountered with the hammer test, and its FRF is directly exported from Siemens Testlab for further processing in MATLAB.

The EMA FRFs are directly identified using the improved Loewner Framework (iLF) [18]. For the OMA configurations, the TVT and AVT time responses are concatenated and processed via the Natural Excitation Technique with the Loewner Framework (NExT-LF) [19]: NExT approximates the system FRF from the response-only cross-spectra, which are then passed to the LF for identification in the usual fashion. The modal parameters obtained from TVT and AVT are compared against the EMA reference. This comparison is presented in Section 3..

3. Results

Before discussing in detail the modal parameters identified from the three tests, it is worth taking a look at the data in the frequency domain. This gives an idea of the response amplitude and potential modes frequency bands (peaks). To carry out this qualitative assessment, the Power Spectral Density (PSD) of the TVT and AVT and the FRF of the hammer test are shown in Figure 5 for each measurement channel, together with the Average Normalised Power Spectral Density (ANPSD) and the average FRF.

It is clear from Figure 5 that the spectral content of all three test configurations is consistent within the identification band. The ANPSD traces from TVT, Figure 5a, exhibit higher overall amplitude than those from AVT, Figure 5b, as expected from the more energetic broadband excitation provided by the taxiway (a brick road in this case) surface imperfections. In both OMA configurations, distinct and repeatable spectral peaks are visible across all sensor channels at approximately 2 Hz, 6 Hz,

[10] https://www.siemens.com/es-es/products/simcenter/physical-testing/scadas/

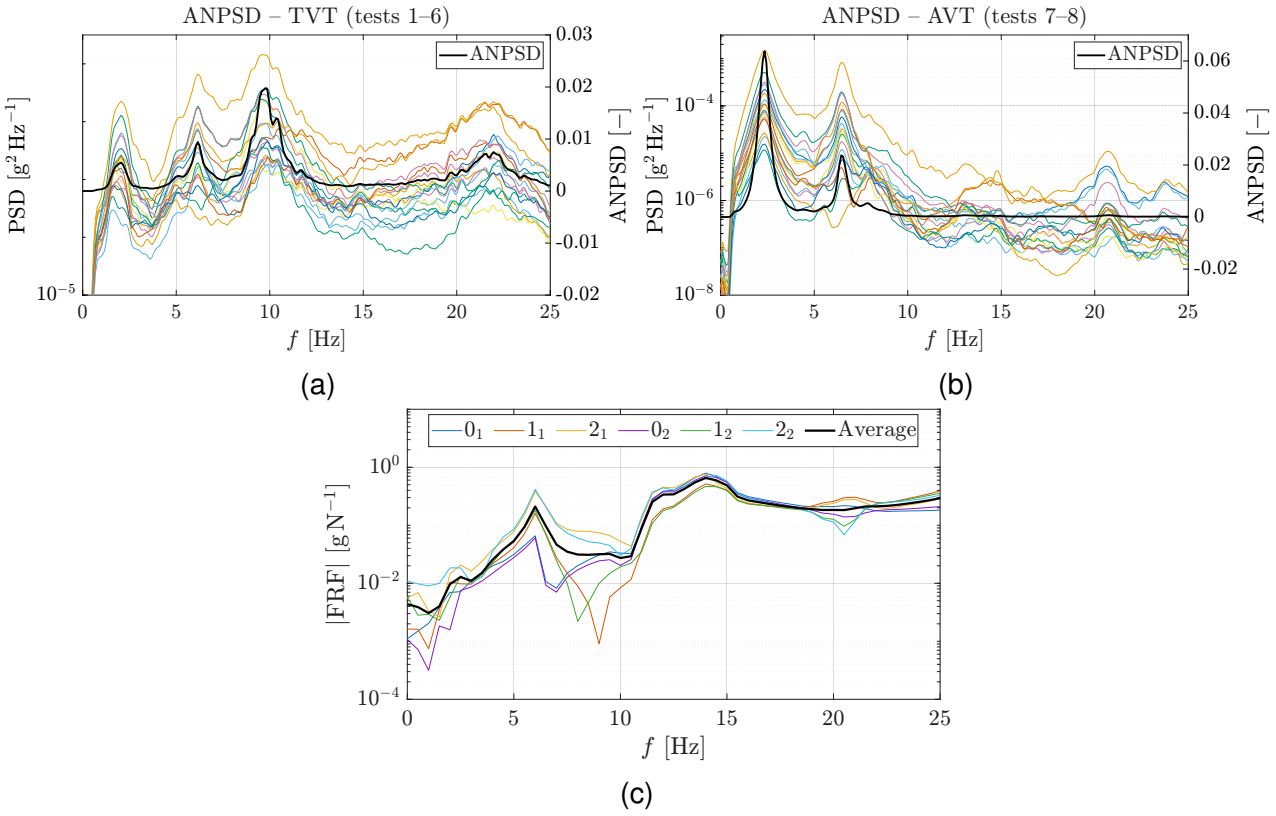


Figure 5 – PSDs and ANPSDs from (a) AVT and (b) TVT, and (c) FRFs and average FRF amplitude from the hammer test.

and in the 10–12 Hz band. The FRF amplitude, Figure 5c, confirms resonance-like features at the same frequency locations, with consistent peak structure across all six measurement channels and the channel average, lending confidence to the subsequent identification procedure.
The modal parameters extracted – natural frequencies f_s in Hz and damping ratio ζ – from the three test configurations are summarised in Table 3, together with the percentage deviations from the EMA reference and the Modal Assurance Criterion (MAC) values computed from the z-direction components of the OMA mode shapes ($\boldsymbol{\phi}_n$) against the EMA reference.

Table 3 – Identified natural frequencies f_n, damping ratios ζ_n, and MAC values from EMA, TVT, and AVT. Percentage deviations from the EMA reference are given in parentheses.

	EMA		**TVT**			**AVT**		
Mode	f_n [Hz]	ζ_n [-]	f_n [Hz]	ζ_n [-]	MAC [-]	f_n [Hz]	ζ_n [-]	MAC [-]
1	2.272	0.010	2.027 (-10.79%)	0.039 (+293.80%)	0.895	2.367 (+4.16%)	0.042 (+327.77%)	0.836
2	6.196	0.016	6.221 (+0.41%)	0.012 (-26.17%)	0.855	6.567 (+5.99%)	0.040 (+146.64%)	0.822
3	11.860	0.026	9.821 (-17.19%)	0.030 (+17.15%)	0.916	—	—	—

Three modes are identified within the 0–25 Hz band. Mode 1 is extracted at $f_n = 2.272$ Hz with $\zeta_n = 1.0\%$ by EMA, while TVT recovers this mode at 2.027 Hz (-10.79%, MAC = 0.895) and AVT at 2.367 Hz (4.16%, MAC = 0.836). Mode 2 is identified at $f_n = 6.196$ Hz; TVT yields 6.221 Hz (0.41%, MAC = 0.855) and AVT 6.567 Hz (5.99%, MAC = 0.822). Mode 3 is identified at $f_n = 11.860$ Hz by EMA and at 9.821 Hz by TVT (-17.19%, MAC = 0.916); AVT does not resolve this mode within the identification band.
The $\boldsymbol{\phi}_n$ obtained from the three configurations are shown in the three-dimensional representation of Figure 6 and in the planar vertical (z-axis) projection of Figure 7.

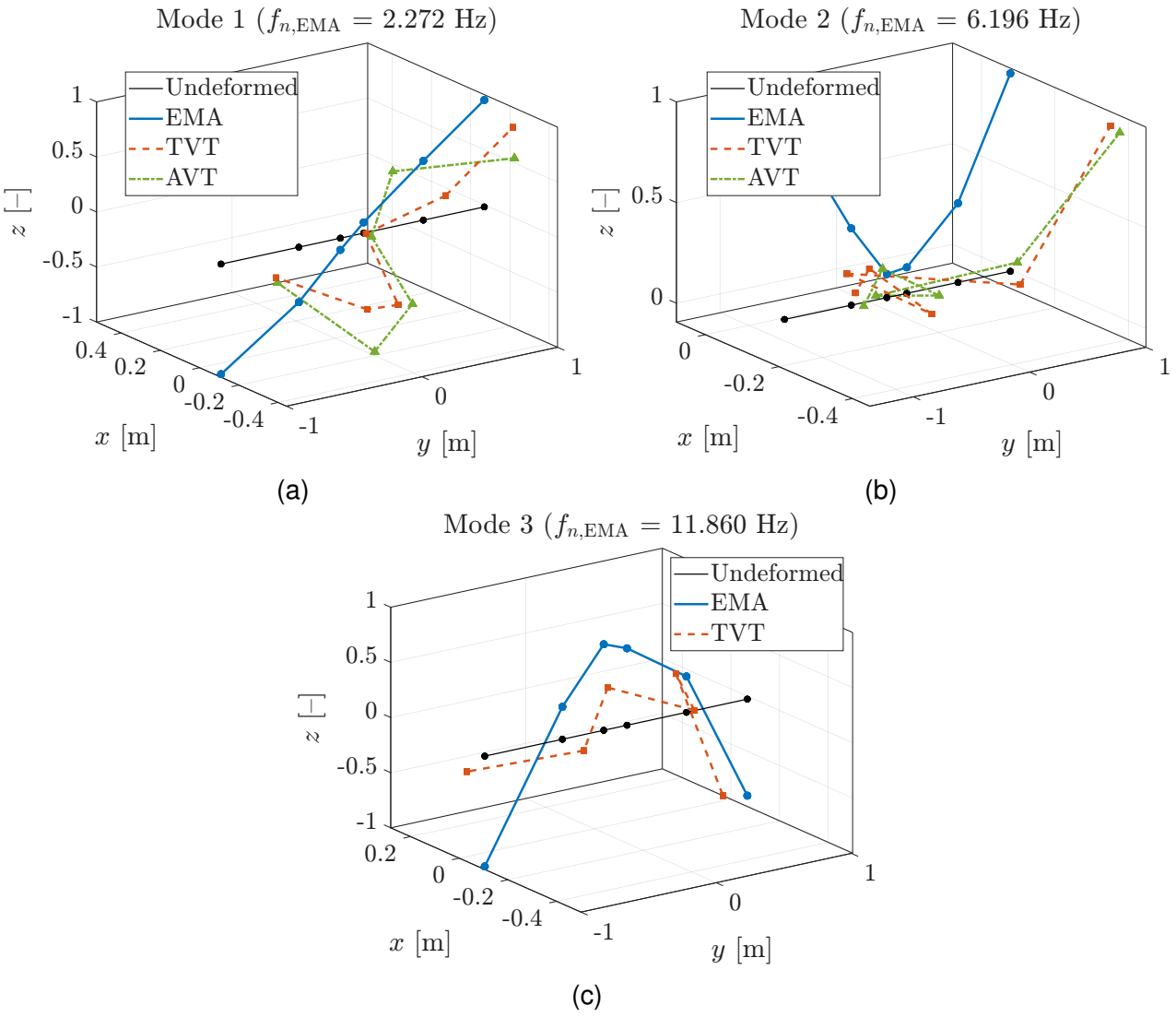


Figure 6 – First three mode shapes identified via EMA, TVT, and AVT.

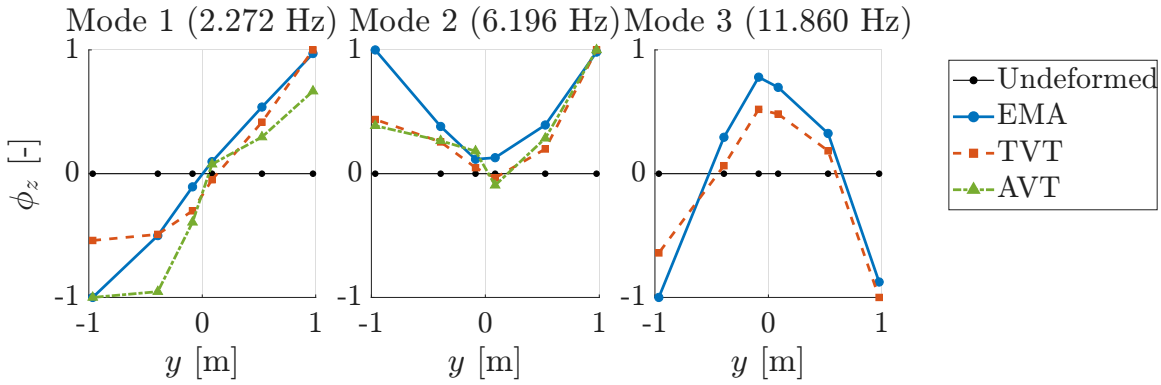


Figure 7 – z-axis modal displacement of the fist three mode shapes identified via EMA, TVT, and AVT.

Mode 1 displays a deformation pattern consistent with the first asymmetric out-of-plane (x-y plane) wing bending, with monotonically increasing displacement amplitude from root to tip on both semi-spans and a node near the fuselage centreline. The three sources are in close agreement on this shape, as reflected in the MAC values. Mode 2 exhibits the first symmetric out-of-plane (x-y plane) wing bending, characterised by a node near mid-span on each semi-span and opposing tip deflections; EMA and TVT agree closely (MAC = 0.855), with AVT showing a slightly larger deviation at the

outermost sensor positions (MAC = 0.822). Mode 3 requires separate consideration. When examined from the vertical displacement components alone, as in Figure 7, the deformation pattern superficially resembles a first bending configuration; however, this attribution is incorrect. The spanwise sensor array captures a secondary bending contribution from a tail assembly mode, as investigated in ongoing work. This interpretation is consistent with the relatively large TVT frequency deviation for this mode (-17.19%), its absence in the AVT results, and the three-dimensional $\boldsymbol{\phi}_3$ of Figure 6c.

4. Discussion

The frequency agreement between the low-cost system and the EMA reference (industrial-grade DAQ) is mode-dependent and warrants individual consideration for each identified mode. Mode 2 is identified at $f_n = 6.196$ Hz by EMA and corresponds to the first symmetric out-of-plane (x-y plane) wing bending of the Ranger airframe. TVT recovers this mode at 6.221 Hz, a deviation of 0.41%, which is below the frequency resolution of the spectral estimate and carries no practical consequence for modal tracking or model correlation. AVT yields 6.567 Hz (5.99%), a larger deviation but consistent with the range reported in OMA-to-EMA comparisons on lightly damped flexible structures [20]. The MAC values for this mode (0.855 from TVT and 0.822 from AVT) confirm that the $\boldsymbol{\phi}_2$ is recovered with acceptable fidelity across all three configurations, and Mode 2 is the most reliably identified mode in this campaign.

Mode 1 presents a wider spread. EMA identifies this mode at $f_n = 2.272$ Hz; TVT yields 2.027 Hz (-10.79%, MAC = 0.895) and AVT 2.367 Hz (4.16%, MAC = 0.836). The AVT result, obtained with the wheels constrained by wooden chocks, is in close agreement with EMA and consistent with the expected first structural mode of the airframe. The TVT deviation is more significant and does not admit a definitive physical explanation within the scope of this study. During the TVT, the Ranger is towed on its undercarriage along the taxiway surface: the tyre-ground contact introduces a compliant support whose stiffness interacts with the lowest structural modes of the airframe [4]. At a frequency as low as 2 Hz, the peak identified from the TVT data may correspond to the first asymmetric wing bending, shifted by the boundary condition, or to a rigid-body bounce or pitch mode of the aircraft-on-undercarriage assembly, or to a coupled mode of both. The spanwise inline sensor layout and the single excitation point do not provide sufficient spatial or modal information to discriminate between these interpretations, and the MAC value of 0.895 is consistent with either: both a shifted structural mode and a rigid-body mode with appreciable wing participation would produce a similar z-direction displacement pattern at these six sensor positions. Resolving this ambiguity would require either a high-fidelity finite element model of the Ranger, or a more complete experimental characterisation of the aircraft low-frequency dynamics, neither of which is within the scope of the present validation campaign.

Mode 3 is identified by EMA at $f_n = 11.860$ Hz, recovered by TVT at 9.821 Hz (-17.19%, MAC = 0.916), and not resolved by AVT. Ongoing experimental campaigns on the Ranger confirm that this mode is dominated by the tail assembly, with the wing spar exhibiting a symmetric bending secondary contribution that the spanwise sensor array captures consistently. The MAC value of 0.916, which is the highest of the three comparisons, reflects this consistency: the projection of the tail mode onto the wing measurement positions is geometrically stable between EMA and TVT, even where the frequency is not recovered accurately. The -17.19% frequency deviation and the failure of AVT to resolve this mode are both expected given the tail-dominated character of the mode: AVT does not provide sufficient energy at the tail to excite it above the noise floor at the wing sensor positions, and TVT, which excites the structure through the undercarriage, may perturb the tail boundary condition in ways that shift the identified frequency (taildragger wheel). The identification of this mode from the wing alone is therefore of limited reliability and should be treated as indicative rather than quantitatively definitive.

Damping estimation from the OMA configurations is, as anticipated, less consistent than the frequency identification. The damping ratios from TVT and AVT exceed the EMA values by factors ranging from approximately two to four, with the largest relative overestimation occurring at Mode 1. This is a known characteristic of OMA-based damping estimates when the WGN excitation assumption is satisfied only approximately [21], and the finite record length introduces bias in the spectral estimate [2]. The EMA damping values (ζ_n between 1.0% and 2.6%) are physically plausible for the

EPO foam and composite construction of the Ranger airframe. For the stated purpose of this validation, the damping overestimation carries limited consequence: the primary quantities of interest for model correlation – f_n and $\boldsymbol{\phi}_n$ – are unaffected by the damping bias.
The system recovers three structural modes of the Ranger with frequency accuracy sufficient for early-stage experimental campaigns and qualitative model correlation, operating within the constraints of a 100 Hz Nyquist ceiling, the absence of traceable sensitivity calibration, and inter-channel timing jitter inherent to the I^2C communication protocol. The 100 Hz ceiling is the principal applicability boundary: for platforms with dominant structural modes above this threshold, the system as configured cannot provide useful spectral data. This is a design constraint of the current implementation rather than a deficiency of the present results, given that all three identified modes fall well within the resolvable band.

5. Conclusions and Future Work

This study validates an affordable, modular DAQ system against industry-standard instrumentation on a small fixed-wing UAV through AVT, TVT, and impact hammer testing. The main findings are:

- The low-cost system (below below €600) reliably identifies the dominant structural modes of the Ranger airframe, with coherent frequency deviations and MAC values across all configurations and test types;
- The first symmetric wing bending at 6.196 Hz is recovered to within 0.41% by TVT and 5.99% by AVT;
- The mode near 2 Hz is recovered by AVT to within 4.16%; the larger TVT deviation cannot be resolved as a shifted structural mode or a rigid-body undercarriage mode without a more complete characterisation of the Ranger low-frequency dynamics;
- The tail-dominated mode at 11.860 Hz is consistently captured via its wing bending secondary contribution, though its identification from the wing array alone is indicative rather than quantitative;
- OMA damping estimates are systematically overestimated relative to EMA, as expected, and do not affect the primary validation claim.

Future work extends the validation to a standard test specimen on a calibrated electrodynamic shaker table, providing a controlled comparison against industrial instrumentation and a direct assessment of noise floor and sensitivity. The modal ambiguity at 2 Hz will be addressed through a finite element model of the Ranger incorporating undercarriage compliance, or through a dedicated low-frequency experimental campaign. The sampling ceiling will be raised through optimised I^2C polling or migration to serial peripheral interface sensors.

Contact Author Email Address

Gabriele Dessena: gdessena@ing.uc3m.es

Acknowledgement

The authors would like to thank Mr Chaoyi Lin Yang, who was responsible for designing the original implementation of the affordable acquisition system. This work is supported by the Madrid Government (*Comunidad de Madrid*, Spain) under the Multiannual Agreement with the Universidad Carlos III de Madrid (IA_aCTRl-CM-UC3M). The first author is supported by grant JDC2024-055593-I funded by MICIU/AEI /10.13039/501100011033 and by ESF+. The Ranger UAV purchase is funded by the Spanish Agencia Estatal de Investigación (AEI) under the Programa Transmisiones, project TIFON (Tecnologías Inteligentes para la Fabricación, el Diseño y las Operaciones en entornos Industriales), grant number PLEC2023-010251. The Department of Aerospace Engineering at UC3M has been accredited as Unit of Excellence “María de Maeztu”, a distinction awarded by the Spanish State Research Agency for the period 01/01/2026-31/12/2031.

Copyright Statement

The authors confirm that they, and/or their company or organization, hold copyright on all of the original material included in this paper. The authors also confirm that they have obtained permission, from the copyright holder of any third party material included in this paper, to publish it as part of their paper. The authors confirm that they give permission, or have obtained permission from the copyright holder of this paper, for the publication and distribution of this paper as part of the ICAS proceedings or as individual off-prints from the proceedings.

References

[1] Gabriele Dessena, Marco Civera, Andrés Marcos, Bernardino Chiaia, and Oscar E. Bonilla-Manrique. Multiple input tangential interpolation-driven damage detection of a jet trainer aircraft. *Aerospace Science and Technology*, 168:111032, 1 2026.

[2] Carlo Rainieri and Giovanni Fabbrocino. *Operational Modal Analysis of Civil Engineering Structures*. Springer New York, 2014.

[3] Bart Peeters, Jan Debille, and Héctor Climent. Modern solutions for ground vibration testing of small, medium and large aircraft. *SAE International Journal of Aerospace*, 1:2008–01–2270, 8 2008.

[4] Marc Böswald, Jan Schwochow, G Jelicic, and Yves Govers. New concepts for ground and flight vibration testing of aircraft based on output-only modal analysis. In W Schober, J Bienert, P F Fernandez, and M L Aenlle, editors, *IOMAC 2017 - 7th International Operational Modal Analysis Conference*, pages 18–34, 2017.

[5] Sanja S. Ivanovic, Mihailo D. Trifunac, and Maria I. Todorovska. Ambient vibration tests of structures - a review. *ISET Journal of Earthquake Technology*, 37:165, 12 2000.

[6] Xinyu Hui, Fan Liu, Xiaodong Li, and Qiaozhi Song. A review of experimental modal analysis methods and their applications in aerospace vehicles. *Advances in Aeronautical Science and Engineering*, 15:16–31, 2024.

[7] Pepito Payet, Damien Ali Hamada Fakra, Rijalalaina Rakotosaona, Marie Hanitriniaina Ratsimba, and Mino Patricia Randrianarison. Design of a highly affordable and reliable data acquisition unit system dedicated to experimental research and education. *Measurement: Journal of the International Measurement Confederation*, 251:117187, 2025.

[8] Alessandro Sabato, Christopher Niezrecki, and Giancarlo Fortino. Wireless MEMS-based accelerometer sensor boards for structural vibration monitoring: A review. *IEEE Sensors Journal*, 17:226–235, 2017.

[9] Erika Delgado Zhagui, Seyedmilad Komarizadehasl, Victor Torralba, Javier Diaz-Rozo, and Jose Turmo. Cost-effective bridge health monitoring via automated operational modal analysis using low-cost adaptable and reliable accelerometers. *Structure and Infrastructure Engineering*, 0:1–16, 6 2025.

[10] Sara Isabel González-Cabrera, Nahum Camacho-Zamora, Sergio-Raul Rojas-Ramirez, Arantxa M. Gonzalez-Aguilar, Marco-Osvaldo Vigueras-Zuniga, and Maria Elena Tejeda del Cueto. Structural vibration analysis of UAVs under ground engine test conditions. *Sensors*, 26:583, 1 2026.

[11] Luigi Buffone, Carmine Manfredi, Kavita Mol S., and Georgios Manganos. Fft real-time low-cost data acquisition system for acquiring wing vibrations displacement. *Research Square*, pages 19, 2026.

[12] Martin Tang, Keith Soal, Marc Böswald, and Yves Govers. Application of gyroscopes for stability monitoring in flutter tests. *Proceedings of the 11th International Operational Modal Analysis Conference, IOMAC 2025*, pages 92–98, 2025.

[13] Marco Civera, Luca Zanotti Fragonara, and Cecilia Surace. Using video processing for the full-field identification of backbone curves in case of large vibrations. *Sensors*, 19:2345, 5 2019.

[14] Chaoyi Lin Yang, Gabriele Dessena, and Oscar E. Bonilla-Manrique. Affordable data collection system for UAVs taxi vibration testing. In *ASME 2026 Aerospace Structures, Structural Dynamics, and Materials Conference*, 2026.

[15] Said Hamada and Claudia P. Moreno. Development of an unmanned aerial vehicle (UAV) research platform for flutter analysis. In *2018 AIAA Atmospheric Flight Mechanics Conference*, pages 1–21, Reston, Virginia, 1 2018. American Institute of Aeronautics and Astronautics.

[16] Luca Zanotti Fragonara, Giosuè Boscato, Rosario Ceravolo, Salvatore Russo, Silvia Ientile, Marica Leonarda Pecorelli, and Antonino Quattrone. Dynamic investigation on the Mirandola bell tower in post-earthquake scenarios. *Bulletin of Earthquake Engineering*, 15:313–337, 2017.

[17] Simone Weber, Thomas Kissinger, Edmond Chehura, Stephen Staines, James Barrington, Kevin Mullaney, Luca Zanotti Fragonara, Ivan Petrunin, Stephen James, Mudassir Lone, and Ralph Tatam. Application of fibre optic sensing systems to measure rotor blade structural dynamics. *Mechanical Systems and Signal Processing*, 158:107758, 9 2021.

[18] Gabriele Dessena and Marco Civera. Improved tangential interpolation-based multi-input multi-output modal analysis of a full aircraft. *European Journal of Mechanics - A/Solids*, 110:105495, 3 2025.

[19] Gabriele Dessena, Marco Civera, and Oscar E. Bonilla-Manrique. Operational modal analysis of aeronautical structures via tangential interpolation. *Aerospace*, 13:378, 4 2026.

[20] Renan Rocha Ribeiro and Rodrigo de Melo Lameiras. Evaluation of low-cost mems accelerometers for shm: Frequency and damping identification of civil structures. *Latin American Journal of Solids and Structures*, 16:1–24, 2019.

[21] Keith Ian Soal, Carsten Thiem, Tobias Meier, Robin Volkmar, Julian Sinske, Yves Govers, and Marc Böswald. Embedded flight vibration testing system for online flutter monitoring of UAVs. In *19th International Forum on Aeroelasticity and Structural Dynamics, IFASD 2022*, Madrid, Spain, 2022.